Solvent Effects on the Hydrodeoxygenation of Propanoic Acid over Pd (111) Model Surfaces

Sina Behtash, Jianmin Lu, Muhammad Faheem, and Andreas Heyden

Department of Chemical Engineering, University of South Carolina,

301 S. Main St., Columbia, South Carolina 29208, USA

Abstract

The effects of liquid water, n-octane, and n-butanol on the hydrodeoxygenation of propanoic acid over Pd (111) model surfaces have been studied from first principles. We developed a microkinetic model for the hydrodeoxygenation and studied the reaction mechanism at a temperature of 473 K. Our model predicts that for all reaction media, decarbonylation pathways are favored over decarboxylation pathways. However, in the presence of polar solvents like water, decarboxylation routes become competitive to decarbonylation routes. The activity of the Pd surface varies as a function of environment as follows: water > n-butanol > octane ≈ gas phase. Finally, a sensitivity analysis of our models suggests that both C-OH and C-H bond cleavages control the overall rate of the catalyst in all environments and are likely activity descriptors for the hydrodeoxygenation of organic acids.

Keywords:

Solvent effects; organic acids; palladium; density functional theory; COSMO; decarbonylation; decarboxylation; microkinetic modeling

1. Introduction

In the past two centuries, fossil fuels have been overused and currently, most countries are extremely dependent on combustion of fossil fuels.[1, 2] Considering the environmental impact of fossil fuel utilization, there is a substantial need for the development of renewable resources such as solar, wind, geothermal, hydropower and biomass for meeting the world's growing energy demand. Biomass is one of the most promising renewable resources and first generation biofuels such as bioethanol and biodiesel have been successfully implemented in the energy system. However, the energy efficiency of 1st generation biofuels is low and there are substantial infrastructure compatibility issues.[3-7] Therefore, there is a need for the development of second-generation biofuels that are identical to current liquid fuels and that can be produced at low cost and high energy conversion efficiency.[8]

Lipid-rich biomass feedstocks, such as vegetable oils, waste fats, and algal lipids are one potential class of raw materials for the production of green fuels. Recently, research efforts[9-11] have been directed to convert these fatty esters and acids into liquid hydrocarbons with the help of a hydroprocess, i.e., the hydrodeoxygenation (HDO) of the feeds over conventional hydrotreating catalysts such as sulfided NiMo/Al_2O_3 and CoMo/Al_2O_3. However, considering the low level of sulfur in biomass and the higher activity of oxygenated feeds versus sulfide feeds conventional hydrotreating catalysts display a short catalyst life time. Also, humin formation and difficulties in separation of carbon oxides from the recycle gas have been reported.[9, 11-13] Consequently, there is an apparent need for new catalysts for the HDO of organic acids and esters. In this context,

we note that the HDO of lipids and triglyceride feedstocks is also relevant to upgrading of the bio-oils obtained from pyrolysis of lignocellulosic biomass.[4, 10, 14]

To rationally design a metal catalyst for the HDO of these feeds, it is necessary to obtain a fundamental understanding of the reaction mechanism for the HDO of organic acids and esters on the catalyst surface.

In our previous studies,[15, 16] two major mechanisms for the HDO, decarbonylation (DCN) and decarboxylation (DCX), of propanoic acids, our model molecule for organic acids, were investigated over Pd (111) model surfaces. The elementary reaction steps involved in the DCN and DCX were identified from first principles and a microkinetic model was developed to determine the dominant pathway and rate-controlling steps under realistic gas phase reaction conditions of 473 K and low, medium, and high partial pressures of hydrogen (0.01, 1 and 30 bar). Our results suggest that the DCN is favored over the DCX and the C-OH bond dissociation of the acid functionality is rate controlling in the DCN mechanism.

Previously, Murzin *et al.* reported[17-19] that for long chain fatty acids over Pd/C catalysts the DCN is favored over the DCX in the presence of hydrogen and only in the absence of hydrogen is the DCX pathway dominant.[20] These results agree with observations from Boda et al.[21] who identified the DCN as the most dominant pathway for the HDO of caprylic acid in a hydrogen atmosphere. However, recently Ford *et al.*[22] reported that even in the presence of hydrogen, the deoxygenation of stearic, lauric, and capric acids follows a decarboxylation mechanism over Pd/C. In this context, it is noted that the experimental studies used different solvents as reaction medium and the effect of solvents on the preferred reaction pathway of the HDO of organic acids remains

unknown. For example, Murzin *et al.* mostly used dodecane as solvent in their studies;[5, 17-19, 23, 24] however, in one of their studies[17], the effect of two different solvents, dodecane and mesitylene, was studied on the decarboxylation of ethyl stearate. According to their results, in dodecane the formation of n-heptadecane was favored while in mesitylene the intermediate product stearic acid is not further reacting to n-heptadecane. Also, it was reported that the initial rates of the decarboxylation are slightly higher in dedocane than in mesitylene. Finally, Hoelderich et al.[25] reported for the catalytic deoxygenation of oleic acid (C18) over Pd/C that the presence of water can change the selectivity towards C17 hydrocarbons by up to 20%.

Considering the lack of fundamental understanding of the effects of solvents on heterogeneous metal catalysts, we investigated in this study the reaction mechanism of the HDO of propanoic acid over Pd (111) from first principles with our novel implicit solvation model for solid surfaces (iSMS).[26]

Since industrial hydrotreatment processing often occurs in a complex liquid environment, we have purposefully selected water, octane and n-butanol as solvents that might mimic this complex environment. In many experimental studies of the HDO of fatty acids, remarkable amounts of water have been produced during the deoxygenation process[6, 20, 22, 24] and also pyrolysis bio-oils contain 25-50 wt% water,[27] justifying the study of water effects on the HDO of organic acids. Similarly, the study of nonpolar octane is justified considering that the chemically similar dedocane is used in most experimental studies of the HDO of fatty acids. Finally, n-butanol has been selected for this study as a solvent with a moderate polarity that might mimic the reaction environments in some bio-oils that contain various alcohols.[27]

2. Methods

2.1 Solvation Model

In this study, the approximate effect of a solvent is investigated with the help of the iSMS method.[26] iSMS is a new approach for modeling reactions at metal-liquid interfaces with implicit solvation models. More information about iSMS and a validation of this method has recently been published by some of us.[26] Basically, the free energy of an adsorbed intermediate on a periodic metal slab at the solid-liquid interface, $G^{liquid}_{surface+\mathrm{int}\,ermediate}$, is defined using a subtraction scheme

$$G^{liquid}_{surface+\mathrm{int}\,ermediate} = G^{vacuum}_{surface+\mathrm{int}\,ermediate} + (G^{liquid}_{cluster+\mathrm{int}\,ermediate} - E^{vacuum}_{cluster+\mathrm{int}\,ermediate}) \quad (1)$$

where, $G^{vacuum}_{surface+\mathrm{int}\,ermediate}$, is the free energy in the absence of a solvent (plane-wave DFT energy of the periodic slab model including vibrational contributions to the free energy), $G^{liquid}_{cluster+\mathrm{int}\,ermediate}$ is the free energy of a metal cluster in the liquid (without explicitly considering vibrational contributions) constructed by removing selected metal atoms from the periodic-slab model and removing the periodic boundary conditions, and $E^{vacuum}_{cluster+\mathrm{int}\,ermediate}$ is the DFT energy of the same cluster in the absence of the solvent. Combinations of COSMO and COSMO-RS[28, 29] implicit solvation models have been used to calculate $G^{liquid}_{cluster+\mathrm{int}\,ermediate}$. COSMO-RS calculations have been performed using COSMOtherm.[30] Thermodynamic properties of the solvents are obtained from the COSMOtherm database, based on the results of quantum chemical COSMO calculations at the BP-TZVP level of theory. For all other structures, COSMO-RS input files have been generated from COSMO calculations at the same level of theory. We note that as a

first approximation we did not include the solvent degrees of freedom in the reaction coordinate.

2.2 DFT calculations

Cluster model DFT calculations were carried out using TURBOMOLE 6.0.[31-33] The Pd (111) cluster model surfaces have been modeled by a two layered cluster with a 5 $\times$5 surface. These structures were constructed by removal of the periodic boundaries from the periodic slabs that were obtained from our previous plane-wave (VASP)[34, 35] calculations.[15] All adsorbates were represented by all-electron TZVP[36-38] basis sets while for Pd we used a relativistic small core potential (ECP) together with a basis set for the valence electrons of same quality as the adsorbates. The Coulomb potential was approximated with the RI-J approximation with auxiliary basis sets[39-41]. Single point energy calculations were performed with a self-consistent field energy convergence criterion of 1.0×10^{-6}. Finally, for each cluster model energy calculations on various spin surfaces were performed to identify the lowest energy spin state for further calculations.

For cluster models in the liquid phase, COSMO calculations were performed on the same spin surface as for the vacuum cluster calculations. The dielectric constant was set to infinity to provide the input for the COSMO-RS calculations. For cavity construction, the default radii-based cavities were used.

2.3 Microkinetic Modeling

For surface reactions, the forward rate constant (k_{for}) of each reaction is calculated as

$$k_{\text{for}} = \frac{k_{\text{B}}T}{h} e^{-\frac{\Delta G^{\ddagger}}{k_{\text{B}}T}} \qquad (2)$$

where k_B is the Boltzmann constant, T denotes the reaction temperature, h is the Planck constant, and $\Delta G^{\ddagger}$ represents the free energy of activation for a specific temperature and reaction environment, i.e., in the presence of solvents, the free energy of activation ($\Delta G^{\ddagger}_{solvent}$) and free energy of reaction ($\Delta G_{rxn\text{-}solvent}$) were calculated as,

$$\Delta G^{\ddagger}_{\text{Solvent}} = \Delta G^{\ddagger}_{\text{Gas}} + G_{TS}(solv) - G_{IS}(solv), \quad (3)$$

and

$$\Delta G_{\text{rxn-solvent}} = \Delta G_{\text{Gas}} + G_{FS}(solv) - G_{IS}(solv) \quad (4)$$

where, $G_{IS}(solv)$, $G_{FS}(solv)$, and $G_{TS}(solv)$ are the solvation energies of the initial, final, and transition states, respectively, that were obtained from the difference in energy of the COSMO-RS and gas-phase cluster calculations, and $\Delta G^{\ddagger}_{\text{Gas}}$ and ΔG_{Gas} are the free energy of activation and reaction under gas phase conditions, respectively. The reverse rate constant (k_{rev}) is calculated from the thermodynamic equilibrium constant K

$$k_{\text{rev}} = \frac{k_{\text{for}}}{K} \quad (5)$$

For an adsorption reaction A(g)+*→A*the rate of adsorption is given by collision theory with a sticking probability of 1 independent of solvent.

$$k_{\text{for}} = \frac{1}{N_0\sqrt{2\pi m_A k_B T}} \quad (6)$$

where N_0 is the number of sites per area (6.766×10^{-20} m^2) and m_A denotes the molecular weight of A. The desorption rate constant is again given by the equilibrium constant, i.e., equation 5.

In the presence of a solvent, the free energy of adsorption for A(g)+*→A* is calculated as,

$$\Delta G_{ads-solvent} = \Delta G_{ads-gas} + G_{A*}(solv) - G_{Pd}(solv) \quad (7)$$

where $\Delta G_{ads-gas}$ is the free energy of adsorption under gas phase conditions and $G_{A*}(solv)$ and $G_{Pd}(solv)$ are as before the solvation energies of the adsorbed molecule A and Pd surface immersed in the solvent, respectively.

With the forward and reverse rate constants defined, rates of the elementary reactions can be expressed by mean-field rate laws. Considering that some of the adsorbed intermediates occupy multiple active sites (the number of occupied sites by each adsorbate is shown in Table1), the rate expressions and steady state molecular balance equations are highly nonlinear. To solve the set of steady state differential reactor equations and to obtain the surface coverages of the intermediates, we used the BzzMath library[42] developed by Buzzi-Ferraris. No assumptions were made regarding rate-limiting steps.

3. Result and discussion

The reaction network investigated in this study was obtained from our previous study on the mechanism of the DCN and DCX of propanoic acid.[15, 16] All of the elementary steps and intermediates involved in DCN and DCX of propanoic acid are shown in Figure 1. The DFT-derived parameters for the reactions are listed in Table 1. Although the DCN and DCX mechanisms are interconnected, key steps in each mechanism are distinguishable. For example, C-OH bond dissociations in propanoic acid and its derivatives (CH_xCH_yCOOH, x=[1,2,3], y=[0,1,2]) form CH_xCH_yCO intermediates which produce CO and C_2 hydrocarbons after a C-C bond dissociation and are therefore key steps in the DCN mechanism. Similarly, key steps unique to the DCX mechanism are

O-H bond dissociations to form CH_xCH_yCOO intermediates followed by C-C cleavage to form CO_2. Also, we grouped C-COOH bond dissociations to form CH_xCH_y and COOH on the surface in the DCX mechanism considering that COOH dissociates on Pd (111) easier to CO_2 and hydrogen than to CO and OH.

(Figure 1)

Table 1 illustrates the effect of solvents on the free energy of reactions and activation barriers of all elementary steps. Solvents can stabilize or destabilize the reactant, product, and transition states.

(Table 1)

For the DCX mechanism, the presence of water affects the following elementary reaction steps most significantly: C-H cleavage in

reaction 30 ($CH_3CH_2COO^{**} + 2^* \rightarrow CH_3CHCOO^{***} + H^*$, $\Delta G_{rxn\text{-}water}$-$\Delta G_{rxn\text{-}gas}$ = -0.17 eV and $\Delta G^{\ddagger\text{-}water}$-$\Delta G^{\ddagger\text{-}Gas}$=-0.24 eV), and

reaction 34 ($CH_3CHCOO^{***} + ^* \rightarrow CH_3CCOO^{***} + H^*$, $\Delta G_{rxn\text{-}water}$-$\Delta G_{rxn\text{-}gas}$ = -0.08 eV and $\Delta G^{\ddagger\text{-}water}$-$\Delta G^{\ddagger\text{-}Gas}$=-0.10 eV), C-$CO_2$ cleavage in

reaction 33 ($CH_3CHCOO^{***} \rightarrow CH_3CH^{**} + CO_2^*$, $\Delta G_{rxn\text{-}water}$-$\Delta G_{rxn\text{-}gas}$ = +0.17 eV and $\Delta G^{\ddagger\text{-}water}$-$\Delta G^{\ddagger\text{-}Gas}$= +0.05 eV) and

reaction 38 ($CH_3CCOO^{***} \rightarrow CH_3C^* + CO_2^* + ^*$, $\Delta G_{rxn\text{-}water}$-$\Delta G_{rxn\text{-}gas}$ = +0.23 eV and $\Delta G^{\ddagger\text{-}water}$-$\Delta G^{\ddagger\text{-}Gas}$=+0.19 eV), and O-H bond cleavage in

reaction 35 ($CH_3CCOOH^{***} + * \rightarrow CH_3CCOO^{***} + H^*$, $\Delta G_{rxn\text{-}water} - \Delta G_{rxn\text{-}gas}$ = -0.11 eV and $\Delta G^{\ddagger\text{-}water} - \Delta G^{\ddagger\text{-}Gas}$=-0.03 eV).

Clearly, in the presence of water, the formation of a (negatively charged) CH_3CCOO species is facilitated and further C-C bond cleavage is inhibited.

For the DCN mechanism, the presence of water affects the following elementary steps most significantly: C-OH bond dissociations become slightly more difficult, e.g., reaction 5 ($CH_3CHCOOH^{**} + * \rightarrow CH_3CHCO^{**} + OH^*$, $\Delta G_{rxn\text{-}water} - \Delta G_{rxn\text{-}gas}$ = +0.08 eV, and $\Delta G^{\ddagger\text{-}water} - \Delta G^{\ddagger\text{-}Gas}$=+0.07) and C-CO bond cleavages become more exergonic, e.g., reaction 3 ($CH_3CH_2CO^{***} \rightarrow CH_3CH_2^* + CO^* + *$, $\Delta G_{rxn\text{-}water} - \Delta G_{rxn\text{-}gas}$ = -0.09 eV) and reaction 8 ($CH_3CHCO^{**} + * \rightarrow CH_3CH^{**} + CO^*$, $\Delta G_{rxn\text{-}water} - \Delta G_{rxn\text{-}gas}$ = -0.07 eV). Also, we observe that C-H dissociates relevant for both DCN and DCX pathways become generally more exergonic, while the corresponding removal of the hydrocarbon pool from the surface, e.g. CHCH +4H $\rightarrow$ CH_3CH_3(g), $\Delta G_{rxn\text{-}water} - \Delta G_{rxn\text{-}gas}$ = +0.12 eV, becomes more endergonic.

Overall, the effect of water is more pronounced for the DCX mechanism than the DCN pathways and while the effect on elementary reaction rates seems to be small, we will show in section 3.1 that the overall effect is quite significant.

Next, the effect of the presence of n-butanol on DCX reactions follows a similar trend to the effect of water with diminished intensity. E.g., C-H bond cleavage in reaction 30 and 34 become more exergonic by -0.06 and -0.07 eV, respectively, while C-CO_2 bond cleavages in e.g. reaction 38 become more endergonic by 0.13 eV (the activation barrier increases by 0.16 eV). So again, production of CH_xCH_yCOO intermediates is facilitated. Also, activation barriers for C-OH bond dissociations such as in reaction 5

($CH_3CHCOOH^{***} + {*} \rightarrow CH_3CHCO^{***} + OH^{*}$) and reaction 13 ($CH_3CCOOH^{***} + {*} \rightarrow CH_3CCO^{***} + OH^{*}$) are increased by 0.11 eV and 0.10 eV, respectively.

Finally, in the presence of n-octane reaction free energies are not significantly affected by the solvent. The most remarkable change occurs in the C-CO bond cleavage of reaction 15 ($CH_2CHCO^{***} + {*} \rightarrow CH_2CH^{***} + CO^{*}$) with $\Delta G_{rxn\text{-}octane} - \Delta G_{rxn\text{-}gas}$ = -0.06 eV and C-CO_2 bond cleavage of reaction 38 ($CH_3CCOO^{***} \rightarrow CH_3C^{*} + CO_2^{*} + {*}$) with $\Delta G_{rxn\text{-}Octane} - \Delta G_{rxn\text{-}gas}$ = +0.08 eV and $\Delta G^{\ddagger\text{-}water} - \Delta G^{\ddagger\text{-}Gas}$=+0.12 eV.

In the following sections the effect of solvents on the turnover frequency (TOF) and the coverage of the most dominant surface species will be studied by mean-field microkinetic modeling.

3.1 Microkinetic modeling

We previously[16] developed mean-field microkinetic models for the reaction mechanism of the DCX and DCN of propanoic acid over Pd (111) surfaces under experimental gas phase conditions. Analysis of the models at a temperature of 473 K and partial pressures of propanoic acid, H_2, CO_2, and H_2O of 1 bar and a CO partial pressure of 0.001 bar (the C_2 product partial pressures were set to zero) suggested that the DCN is slightly preferred over the DCX. Also, the mechanism and turnover frequencies (TOF) were found to be not sensitive to the partial pressures of H_2O and CO_2, as well as CO (in the range of 10^{-4} to 10^{-1} bar). The most abundant surface intermediates under gas phase conditions were adsorbed hydrogen, CO, and CH_3C. We note that we used a method similar to Grabow *et al.*[43] for determining coverage dependent adsorption energies of CO, H, and CH_3C.

In this study, we developed a microkinetic model for all elementary steps involved in both the DCX and DCN networks (previously the networks were studied independently) with forward and reverse rate parameters shown in Table 2.

(Table 2)

Again, all calculations were carried out at 473K which is a typical experimental temperature.[5, 17-20, 23, 44] We selected partial pressures of propanoic acid, water, and CO_2 of 1 bar and a CO partial pressure of 0.1 bar which is larger than in our previous study and corresponds to a condition of about 10% conversion. Additionally, all simulations were carried out under low (0.001 bar) and medium (1 bar) hydrogen partial pressures to investigate the effect of hydrogen partial pressure on the reaction mechanism in the presence of various solvents. For simplicity, all results corresponding to the low partial pressure of hydrogen environment are displayed in this paper in [ ] bracket next to the results of the medium hydrogen partial pressure. Finally, for all simulations in all solvents we employed the same coverage dependent adsorption energies of CO, H, and CH_3C as in our previous study.[16]

Figure 2 illustrates the turnover frequencies of all elementary steps under gas-phase conditions. The overall TOF was calculated to be 1.30×10^{-6} s^{-1} at medium hydrogen partial pressure [2.13×10^{-5} s^{-1} at low hydrogen partial pressure]. The TOF of the DCN pathways are 1.28×10^{-6} s^{-1} [2.11×10^{-5} s^{-1}] and the TOF of the DCX pathways are 2.26×10^{-8} s^{-1} [1.43×10^{-7} s^{-1}], illustrating that the rate of the DCN is two orders of magnitude higher than the DCX. Next, we find the dominant reaction mechanism to be independent of the partial pressure of hydrogen to involve propanoic acid to undergo

three dehydrogenation steps of α and β-carbons to form CHCHCOOH, followed by C-OH cleavage, and C-CO bond dissociation to produce C_2 products (CH_3CH_2COOH → $CH_3CHCOOH$ → $CH_2CHCOOH$ → CHCHCOOH → CHCHCO → CHCH). 31% [43% in the low hydrogen scenario] of the surface was free of adsorbed intermediates and the most abundant surface species are adsorbed hydrogen, CO, and CH_3C with coverages of 23% [7%], 34% [35%], and 12% [14%], respectively.

In the following, the effects of various solvent on reaction mechanism and TOF of the DCN and DCX mechanism will be discussed.

(Figure 2)

3.1.1 Liquid water effects

Water itself is one of the products of our reaction network as well as a relevant reaction environment. In the presence of water, calculations were again carried out at 473 K and chemical potentials corresponding to the same gas phase partial pressures of the gas-phase study described above (except for water). For the water chemical potential we assumed gas-liquid equilibrium, i.e., the water partial pressure is computed as,

$$x_{water} f^{L}_{water} = y_{water} P_{total} = P_{water} \qquad (8)$$

where x_{water} is the mole fraction of water in the solvent mixture, f^{L}_{water} is the fugacity of pure water at 473 K, y_{water} is the mole fraction of water in the vapor, P_{tot} is the total pressure of the system, and P_{water} denotes the partial pressure of water. Assuming the solution is dilute, the mole fraction of water in solution (x_{water}) is 1. Also, the fugacity of

pure water at 473 K can be obtained from a steam table[45] and is f_{water}^{L}=14.17 bar. Finally, the partial pressure of water is calculated to be 14.17 bar and this value was used for all further microkinetic simulations (for other solvents and gas phase simulations the water partial pressure was set to 1 bar).

In liquid water, we find again that the most abundant surface species are H, CO, CH_3C and free (water covered) sites with coverages of 22% [7%], 35% [38%], 13% [14%], and 30% [41%], respectively. The overall TOF increased by a factor of 28 [31 in the low hydrogen partial pressure scenario] from $TOF_{overall\text{-}gas}=1.30\times10^{-6}$ s^{-1} [2.13×10^{-5} s^{-1}] to $TOF_{overall\text{-}water}=3.62\times10^{-5}$ s^{-1} [6.61×10^{-4} s^{-1}]. The calculated TOFs for all elementary steps are shown in Figure 3.

As we expected, the DCX is significantly more affected by liquid water than the DCN. TOFs of DCX pathways increased by more than two orders of magnitude from $TOF_{DCX\text{-}gas}= 2.26\times10^{-8}$ s^{-1} [1.43×10^{-7} s^{-1}] to $TOF_{DCX\text{-}water}= 6.21\times10^{-6}$ s^{-1} [7.86×10^{-5} s^{-1}] while the TOFs of DCN pathways only increased by one order of magnitude from $TOF_{DCN\text{-}gas}= 1.28\times10^{-6}$ s^{-1} [2.11×10^{-5} s^{-1}] to $TOF_{DCN\text{-}water}= 3.00\times10^{-5}$ s^{-1} [2.94×10^{-4} s^{-1}]. Clearly, in liquid water DCX and DCN pathways are very competitive and our calculations suggest that the DCN is dominant with a TOF_{DCN} to TOF_{DCX} ratio of only 4.8 [3.7] which is most likely within the accuracy of our calculations and models. As a result of the dominance of the DCN, the predicted most favorable pathway does not change in the presence of water from our previous gas phase results. The dominant DCX pathway starts with a dehydrogenation step of the α-carbon to form $CH_3CHCOOH$, followed by O-H bond cleavage and further α-carbon dehydrogenation prior to C-CO_2

bond cleavage and hydrogenation to C_2 products (CH_3CH_2COOH → $CH_3CHCOOH$ → CH_3CHCOO → CH_3CCOO → CH_3C → → CH_3CH_3 / CH_2CH_2).

(Figure 3)

3.1.2 Liquid octane effects

Simulations in liquid octane were performed at reaction conditions similar to the gas-phase simulations. The results of our DFT calculations in liquid octane already suggested that octane has only a minor effect on the reaction parameters and consequently, we did not expect any significant effect on the reaction mechanism and overall TOF in comparison to our gas-phase results. Indeed, Figure 4 illustrates that the DCX and DCN mechanisms are hardly affected and the dominant pathway remains under all studied hydrogen environments: CH_3CH_2COOH → $CH_3CHCOOH$ → $CH_2CHCOOH$ → CHCHCOOH → CHCHCO → CHCH. Also, the overall TOF values in the presence and absence of Octane are almost the same ($TOF_{overall\text{-}Octane}=1.77\times10^{-6}$ s^{-1} [2.23×10^{-5} s^{-1}] vs. $TOF_{overall\text{-}gas}=1.30\times10^{-6}$ s^{-1}[2.13×10^{-5} s^{-1}]). The most abundant species were free sites, CO, H, and CH_3C with surface coverages of 30% [42%], 35% [37%], 23% [7%], and 13% [13%], respectively.

(Figure 4)

3.1.3 Liquid n-butanol effects

Simulations in liquid n-butanol were performed at reaction conditions similar to the gas-phase simulations. The overall TOF was calculated to be $5.75\times10^{-6}s^{-1}$ [1.23×10^{-4} s^{-1}] which is relatively larger than the gas phase and octane TOFs and smaller than the water TOFs. The dominant mechanism at both low and medium hydrogen partial pressures is again the DCN with the most favorable pathways staying the same as under gas-phase conditions. However, in the presence of n-butanol, the TOF of the DCX increased by a factor of 28 [47] from $TOF_{DCX\text{-}gas}=2.26\times10^{-8}$ s^{-1} [1.43×10^{-7} s^{-1}] to $TOF_{DCX\text{-}Butanol}=6.26\times10^{-7}$ s^{-1} [6.76×10^{-6} s^{-1}]. Figure 5 illustrates that the dominant pathway of the DCX is similar to the pathway in liquid water (CH_3CH_2COOH → $CH_3CHCOOH$ → CH_3CHCOO → CH_3CCOO → CH_3C → → CH_3CH_3 / CH_2CH_2). The most abundant surface species are free sites, CO, H, and CH_3C with the coverages of 30% [42%], 35% [37%], 22% [7%], and 13% [13%], respectively.

As already predicted from the solvation free energies, in the presence of n-butanol the TOFs are similar but lower than the TOFs in liquid water. We observe that as the polarity of the solvents increases from octane to n-butanol to water, the DCX and to a lower degree the DCN are facilitated such that the overall TOF in the presence of liquid octane is about the same as in the gas-phase, increases for butanol by a factor of 4.4 [5.8] and finally increases for water by a factor of 27.9 [31.1].

(Figure 5)

3.2 Apparent activation barrier, reaction orders, and sensitivity analysis

Apparent activation barriers were computed in the temperature range of 423 to 523 K in all reaction environments and hydrogen partial pressures.

$$E_a = RT^2\left(\frac{\partial \ln(r)}{\partial T}\right)_{p_i} \tag{9}$$

Next, the reaction order with respect to hydrogen was calculated at 473 K for the low hydrogen partial pressure in the range of 0.0005 to 0.002 bar and for the medium hydrogen partial pressure in the range of 0.5 to 2 bar using equation 10. Similarly, the reaction order of propanoic acid and CO were calculated at 473 K and a pressure range of 0.5 to 2 bar and 0.0001 to 1 bar, respectively.

$$\alpha_i = \left(\frac{\partial \ln(r)}{\partial \ln(p_i)}\right)_{T,p_{j\neq i}} \tag{10}$$

Finally, Campbell's degrees of rate and thermodynamic control[46-48], X_{RC} and X_{TRC}, were used to determine the rate controlling steps and intermediates in the mechanism. Rate controlling steps and intermediates are those transition states and intermediates that most strongly influence the reaction rate and are potential activity descriptors.

$$X_{\mathrm{RC},i} = \frac{k_i}{r}\left(\frac{\partial r}{\partial k_i}\right)_{K_i,k_j\neq k_i} \quad , \quad X_{\mathrm{TRC},n} = \frac{1}{r}\left(\frac{\partial r}{\partial\left(\frac{-G_n^0}{RT}\right)}\right)_{G_{m\neq n}^0, G_i^{0,\mathrm{TS}}} \tag{11}$$

where r is the overall rate of reaction, k_i is the forward rate constant for step i, K_i equilibrium constant for step i, R is the gas constant, T denotes the reaction temperature, and G_n^0 is the free energy of adsorbate n.

3.2.1 Gas phase

Medium partial pressure of hydrogen (p_{H2} = 1 bar)

At a reaction temperature of 473 K and a hydrogen partial pressure of 1 bar, our model predicts an apparent activation energy of 0.84 eV in a gas phase environment. The reaction order with respect to propanoic acid is +1.0, with respect to CO it is +0.31, and finally with respect to H_2 it is -0.80. These results are in good agreement to our previous study[16]. Next, the C-OH bond dissociation as well as α- and β-carbon dehydrogenation steps are found to be rate-controlling. For example, the X_{RC} values for the C-OH cleavage reactions 17 (CHCHCOOH*** + 2*→ CHCHCO**** + OH*), reaction 5 ($CH_3CHCOOH$** + *→ CH_3CHCO** + OH*), and reaction 11 ($CH_2CHCOOH$*** + *→ CH_2CHCO*** + OH*) were calculated to be 0.49, 0.23, and 0.17, respectively. The X_{RC} value of the dehydrogenation of the α-carbon in propanoic acid (reaction 2) is rate controlling with X_{RC} = 0.32 and the first and second dehydrogenation steps of the β-carbon in $CH_3CHCOOH$ are rate controlling with X_{RC} = 0.09 (reaction 6) and X_{RC} = 0.06 (reaction 12), respectively. We note that the sum of the degree of rate control is larger one due to numerical inaccuracies of our nonlinear equation solver; however, the trends should not be affected by these numerical issues. Also, these results are in agreement with previous calculations[49, 50] from Pallassana and Neurock and Olcay et al. who found that the C-OH bond cleavage is rate controlling for the HDO of acetic acid. Our model in addition highlights the importance of dehydrogenation steps. Finally, the thermodynamic rate control analysis suggests that the adsorption free energy of H* and CO* have a significant effect on the overall rate with X_{TRC} = -1.52 and 0.21, respectively, such that destabilizing the adsorbed hydrogen or stabilizing CO improves the overall reaction rate.

CO is generally known to be a surface poison; however, due to repulsive lateral interactions with adsorbed H* and the negative reaction order with respect to hydrogen we observe that destabilizing adsorbed H* is more important than stabilizing CO*. We are currently in the process of testing this hypothesis experimentally.

Low partial pressure of hydrogen (p_{H2} = 0.001bar)

At a low partial pressure of hydrogen, the coverage of hydrogen drops from 23% (p_{H2} = 1 bar) to 7%. Also, the available free sites increased from 31% to 42%. However, the coverage of CO is not significantly affected and in fact, slightly increases from 34% to 35%. Now, the thermodynamic rate control analysis suggests that destabilizing both CO* and H* improves the overall rate with X_{TRC} = -0.03 and -0.33, respectively. Also, the dehydrogenation of the α-carbon in propanoic acid is clearly the most rate controlling step with X_{RC} = 1.0.C-OH bond dissociation becoming less important with X_{RC} = 0.05 for reaction 17.

Finally, our model predicts an apparent activation barrier of 0.62 eV (which is 0.22 eV lower than at a hydrogen partial pressures of 1bar) and orders of reaction for CO and H_2 that are close to zero (i.e., -0.02 and -0.13, respectively). The calculated propanoic acid reaction order is again 1.

3.2.2 Liquid water

Water - Medium partial pressure of hydrogen (P_{H2} = 1 bar)

In the presence of liquid water and at a hydrogen partial pressure of 1 bar, C-OH bond dissociations are in agreement with our gas-phase simulations the most rate controlling steps (e.g., X_{RC} = 0.43 for reaction 17, X_{RC} = 0.28 for reaction 11, and X_{RC} =

0.09 for reaction 5). Next, α and β-carbon dehydrogenation steps have some influence on the net reaction rate (X_{RC} = 0.25 for reaction 2, X_{RC} = 0.09 for reaction 6, and X_{RC} = 0.05 for reaction 12). As discussed above, in the presence of water the DCX becomes competitive with the DCN. As a result, our sensitivity analysis finds that O-H and C-H cleavage steps involved in the DCX become rate controlling, e.g., reaction 31 ($CH_3CHCOOH^{**} + * \rightarrow CH_3CHCOO^{**} + H^*$) with X_{RC} = 0.03, reaction 34 ($CH_3CHCOO^{***} + * \rightarrow CH_3CCOO^{***} + H^*$) with X_{RC} = 0.06, and reaction 30 ($CH_3CH_2COO^{**} + 2^* \rightarrow CH_3CHCOO^{***} + H^*$) with X_{RC} = 0.05. Thermodynamic rate control analysis suggests again that destabilizing H* and stabilizing CO* improves the reaction rate with X_{TRC} = -1.55 and +0.18, respectively. Finally, the reaction orders with respect to CO, hydrogen, and propanoic acid are -0.77, 0.28 and 1.0, respectively, and the apparent activation energy is calculated as 0.68 eV which is 0.16 eV smaller than the gas-phase activation barrier.

Water - Low partial pressure of hydrogen (P_{H2} = 0.001 bar)

At a hydrogen partial pressure of 0.001 bar, dehydrogenation steps of the α-carbon of propanoic acid are the most rate controlling steps, e.g., for reaction 2 X_{RC} = 0.79 and for reaction 30 X_{RC} = 0.11, while the C-OH bond dissociation in reaction 17 becomes less influential with X_{RC} = 0.08. Again, in agreement with the gas-phase simulations thermodynamic rate control analysis suggests that destabilizing both CO* and H* improves the reaction rate with X_{TRC} = -0.03 and X_{TRC} = -0.39. Finally, the reaction orders of propanoic acid, CO and H_2 are calculated to be 1.0, -0.02, and -0.17 respectively, and the apparent activation barrier is predicted as 0.48 eV.

3.2.3 Liquid octane

n-Octane - Medium partial pressure of hydrogen (P_{H2} = 1 bar)

In the presence of liquid octane changes in the reaction parameters, TOF, and surface coverages are negligible in comparison to our gas-phase results. As a result, our model predicts an activation barrier of 0.84 eV and reaction orders of propanoic acid, H_2 and CO of 1.0, -0.74, and 0.28, respectively, that are very similar to our gas-phase simulations. Finally, C-OH bond dissociations in reaction 17, 11, and 5 are most rate controlling with X_{RC}'s of 0.48, 0.20 and 0.20, respectively. Next, dehydrogenation steps in reaction 2, 6, and 12 (X_{RC} = 0.34, X_{RC} = 0.09, and X_{RC} = 0.06, respectively) and the stability of adsorbed CO* and H* (X_{TRC} = +0.19 and X_{TRC} = -1.44, respectively) have some influence on the overall reaction rate.

n-Octane – Low partial pressure of hydrogen (P_{H2}=0.001 bar)

At a hydrogen partial pressure of 0.001 bar, the dehydrogenation of the α-carbon of propanoic acid (reaction 2) is most rate controlling (X_{RC}=0.89) and the C-OH bond dissociation in reaction 17 is less influential (X_{RC}=0.05). The thermodynamic degree of rate control for CO* and H* are calculated as -0.03 and -0.34, respectively. Finally, very similar to our gas-phase simulations our model predicts an apparent activation barrier of 0.63 eV and propanoic acid, hydrogen and CO reaction orders of 1.0, -0.15, and -0.02 respectively.

3.2.4 Liquid n-butanol

n-Butanol – Medium partial pressure of hydrogen (P_{H2} =1 bar)

The presence of liquid n-butanol leads to qualitatively similar changes to the reaction mechanism and TOF as the presence of liquid water. C-OH bond dissociations are still the most rate controlling steps, i.e., reaction 17 (X_{RC} = 0.48), reaction 11 (X_{RC} =0.27), and reaction 5 (X_{RC} =0.15), followed by α and β-carbon dehydrogenations (reaction 2 with X_{RC} = 0.25, reaction 6 with X_{RC} = 0.10, reaction 12 with X_{RC} = 0.06, and reaction 34 with $X_{RC\text{-}R34}$=0.06) and O-H bond dissociations relevant for the DCX (reaction 31 with X_{RC} = 0.02 and reaction 30 with X_{RC} = 0.01). Thermodynamic rate control analysis suggests again that destabilizing H* and stabilizing CO* improves the reaction rate with X_{TRC} = -1.61 and +0.21, respectively. Finally, the reaction orders with respect to propanoic acid, H_2 and CO are 1.0, -0.82, and +0.31, respectively, and the apparent activation energy is calculated as 0.76 eV which is 0.1 eV smaller than the gas-phase activation barrier and 0.08 eV larger than the activation barrier in liquid water.

n-Butanol – Low partial pressure of hydrogen (P_{H2} = 0.001 bar)

At a hydrogen partial pressure of 0.001 bar, dehydrogenation steps of the α-carbon in propanoic acid are the most rate controlling steps, e.g., for reaction 2 X_{RC}= 0.80 and for reaction 30 X_{RC} = 0.06, while the C-OH bond dissociation in reaction 17 becomes less influential with X_{RC} = 0.10. Again, in agreement with both water and gas-phase simulations thermodynamic rate control analysis suggests that destabilizing both CO* and H* improves the reaction rate with X_{TRC} = -0.03 and X_{TRC} = -0.41. Finally, the reaction orders of propanoic acid, CO and H_2 are calculated to be 1.0, -0.01, and -0.18, respectively, and the apparent activation barrier is predicted to be 0.47 eV which is essentially equivalent to the activation barrier in liquid water.

4. Conclusion

The effect of three different solvents, liquid water, n-octane, and n-butanol has been investigated on the decarbonylation and decarboxylation of propanoic acid over Pd (111) model surfaces with the help of periodic DFT calculations, COSMO-RS implicit solvation with iSMS scheme and microkinetic modeling. We developed mean-field microkinetic models for each solvent at a temperature of 473 K and low (0.001 bar) and medium (1 bar) hydrogen partial pressures. Under all conditions is the decarbonylation the dominant HDO mechanism with the most favored pathway following dehydrogenation steps prior to C-OH and C-CO bond cleavages, i.e., CH_3CH_2COOH → $CH_3CHCOOH$ → $CH_2CHCOOH$ → CHCHCOOH → CHCHCO → CHCH → → CH_3CH_3 / CH_2CH_2. In nonpolar solvents such as octane, we do not observe any significant solvent effects on the elementary surface reactions and overall turnover frequency. However, with increasing polarity of the solvent, e.g., n-butanol and protic water, does the overall turnover frequency increase by up to a factor 30 from the gas-phase turnover frequency. Also, the apparent activation barrier decreases in the presence of liquid water by up to 0.16 eV. Another significant effect of a polar solvent such as water is that it stabilizes key intermediates in the decarboxylation mechanism such that the decarboxylation rate increases by two orders of magnitude and the decarbonylation and decarboxylation pathways become essentially competitive. Finally, a sensitivity analysis suggests that in all reaction environments and at a low hydrogen partial pressure is the dehydrogenation of α-carbon in propanoic acid most rate controlling. With increasing hydrogen partial pressure, the C-OH bond dissociation becomes most rate controlling and the importance of C-H bond cleavages is diminished. As a result, both C-

H and C-OH bond dissociations are likely important activity descriptors for a future computational catalyst discovery and design study.

Acknowledgements

We gratefully acknowledge the financial support from the National Science Foundation (CHE-1153012) and in part from the U.S. Department of Energy, Office of Basic Energy Sciences, Chemical Sciences Division under Contract DE-SC0007167. Computational resources have been provided by the National Energy Research Scientific Computing Center (NERSC) which is supported by the Office of Science of the U.S. Department of Energy and in part by XSEDE under grant number TG-CTS090100. Finally, computing resources from the USC NanoCenter and USC's High Performance Computing Group are gratefully acknowledged.

References

1. BP Statistical Review of World Energy, June 2012, URL: http://www.bp.com/assets/bp_internet/globalbp/globalbp_uk_english/reports_and_publications/statistical_energy_review_2011/STAGING/local_assets/pdf/statistical_review_of_world_energy_full_report_2012.pdf.
2. EIA Annual Energy Review 2010, U.S. Energy Information Administration, October 2011, URL: http://www.eia.gov/totalenergy/data/annual/pdf/aer.pdf.
3. M. J. Ramos, C. M. Fernandez, A. Casas, L. Rodriguez and A. Perez, *Bioresource Technology*, 2009, **100**, 261-268.
4. J. C. Serrano-Ruiz and J. A. Dumesic, *Energy & Environmental Science*, 2011, **4**, 83-99.
5. S. Lestari, P. Maki-Arvela, K. Eranen, J. Beltramini, G. Q. M. Lu and D. Y. Murzin, *Catalysis Letters*, 2010, **134**, 250-257.
6. J. Monnier, H. Sulimma, A. Dalai and G. Caravaggio, *Applied Catalysis A-General*, 2010, **382**, 176-180.
7. G. Knothe, *Fuel Processing Technology*, 2005, **86**, 1059-1070.
8. J. Regalbuto, *Computers & Chemical Engineering*, 2010, **34**, 1393-1396.
9. G. W. Huber, P. O'Connor and A. Corma, *Applied Catalysis A-General*, 2007, **329**, 120-129.
10. B. Donnis, R. G. Egeberg, P. Blom and K. G. Knudsen, *Topics in Catalysis*, 2009, **52**, 229-240.
11. D. Kubicka, P. Simacek and N. Zilkova, *Topics in Catalysis*, 2009, **52**, 161-168.
12. R. Weingarten, G. A. Tompsett, W. C. Conner and G. W. Huber, *Journal of Catalysis*, 2011, **279**, 174-182.
13. S. G. Wettstein, D. M. Alonso, Y. X. Chong and J. A. Dumesic, *Energy & Environmental Science*, 2012, **5**, 8199-8203.
14. M. Stocker, *Angewandte Chemie-International Edition*, 2008, **47**, 9200-9211.
15. J. M. Lu, S. Behtash and A. Heyden, *Journal of Physical Chemistry C*, 2012, **116**, 14328-14341.
16. J. Lu, S. Behtash, M. Faheem and A. Heyden, *Journal of Catalysis*, 2013, **305**, 56-66.
17. P. Maki-Arvela, I. Kubickova, M. Snare, K. Eranen and D. Y. Murzin, *Energy & Fuels*, 2007, **21**, 30-41.
18. I. Simakova, O. Simakova, P. Maki-Arvela and D. Y. Murzin, *Catalysis Today*, 2010, **150**, 28-31.
19. I. Simakova, B. Rozmyslowicz, O. Simakova, P. Maki-Arvela, A. Simakov and D. Y. Murzin, *Topics in Catalysis*, 2011, **54**, 460-466.
20. B. Rozmyslowicz, P. Maki-Arvela, A. Tokarev, A. R. Leino, K. Eranen and D. Y. Murzin, *Industrial & Engineering Chemistry Research*, 2012, **51**, 8922-8927.
21. L. Boda, O. Gyorgy, H. Solt, L. Ferenc, J. Valyon and A. Thernesz, *Applied Catalysis A-General*, 2010, **374**, 158-169.
22. J. P. Ford, J. G. Immer and H. H. Lamb, *Topics in Catalysis*, 2012, **55**, 175-184.
23. S. Lestari, P. Maki-Arvela, I. Simakova, J. Beltramini, G. Q. M. Lu and D. Y. Murzin, *Catalysis Letters*, 2009, **130**, 48-51.

24. J. G. Immer, M. J. Kelly and H. H. Lamb, *Applied Catalysis A-General*, 2010, **375**, 134-139.
25. M. Arend, T. Nonnen, W. F. Hoelderich, J. Fischer and J. Groos, *Applied Catalysis A-General*, 2011, **399**, 198-204.
26. M. Faheem, S. Suthirakun and A. Heyden, *Journal of Physical Chemistry C*, 2012, **116**, 22458-22462.
27. T. P. Vispute, H. Y. Zhang, A. Sanna, R. Xiao and G. W. Huber, *Science*, 2010, **330**, 1222-1227.
28. A. Klamt, *Journal of Physical Chemistry*, 1995, **99**, 2224-2235.
29. A. Klamt, V. Jonas, T. Burger and J. C. W. Lohrenz, *Journal of Physical Chemistry A*, 1998, **102**, 5074-5085.
30. A. Klamt, *COSMO-RS: From Quantum Chemistry to Fluid PhaseThermodynamics and Drug Design*, Elsevier Science, 2005.
31. R. Ahlrichs, M. Bar, M. Haser, H. Horn and C. Kolmel, *Chemical Physics Letters*, 1989, **162**, 165-169.
32. O. Treutler and R. Ahlrichs, *Journal of Chemical Physics*, 1995, **102**, 346-354.
33. TURBOMOLE V6.0 2009, a development of University of Karlsruhe and Forschungszentrum Karlsruhe GmbH, 1989–2007, TURBOMOLE GmbH, since 2007.
34. G. Kresse and J. Hafner, *Physical Review B*, 1993, **47**, 558-561.
35. G. Kresse and J. Furthmuller, *Computational Materials Science*, 1996, **6**, 15-50.
36. F. Weigend, M. Haser, H. Patzelt and R. Ahlrichs, *Chemical Physics Letters*, 1998, **294**, 143-152.
37. F. Weigend and R. Ahlrichs, *Physical Chemistry Chemical Physics*, 2005, **7**, 3297-3305.
38. F. Weigend, *Physical Chemistry Chemical Physics*, 2006, **8**, 1057-1065.
39. K. Eichkorn, O. Treutler, H. Ohm, M. Haser and R. Ahlrichs, *Chemical Physics Letters*, 1995, **242**, 652-660.
40. K. Eichkorn, F. Weigend, O. Treutler and R. Ahlrichs, *Theoretical Chemistry Accounts*, 1997, **97**, 119-124.
41. M. Von Arnim and R. Ahlrichs, *Journal of Computational Chemistry*, 1998, **19**, 1746-1757.
42. G. Buzzi-Ferraris, *"BzzMath: Numerical libraries in C++", Politecnico di Milano:* www.chem.polimi.it/homes/gbuzzi.
43. L. C. Grabow, B. Hvolbaek and J. K. Norskov, *Topics in Catalysis*, 2010, **53**, 298-310.
44. P. Maki-Arvela, B. Rozmyslowicz, S. Lestari, O. Simakova, K. Eranen, T. Salmi and D. Y. Murzin, *Energy & Fuels*, 2011, **25**, 2815-2825.
45. J. M. Smith, H. C. Van Ness and M. M. Abbott, *Introduction to chemical engineering thermodynamics*, McGraw-Hill, 2005.
46. C. T. Campbell, *Topics in Catalysis*, 1994, **1**, 353-366.
47. C. T. Campbell, *Journal of Catalysis*, 2001, **204**, 520-524.
48. C. Stegelmann, A. Andreasen and C. T. Campbell, *Journal of the American Chemical Society*, 2009, **131**, 8077-8082.
49. V. Pallassana and M. Neurock, *Journal of Catalysis*, 2002, **209**, 289-305.
50. H. Olcay, L. J. Xu, Y. Xu and G. W. Huber, *ChemCatChem*, 2010, **2**, 1420-1424.

Table 1. Reaction free energies in eV for all elementary reaction steps in the hydro-deoxygenation of propanoic acid over Pd (111) model surfaces at a temperature of 473 K.

#	Reaction	Gas		Water		Octane		Butanol	
		ΔG_{rxn}	$\Delta G^{\ddagger}$	ΔG_{rxn}	$\Delta G^{\ddagger}$	ΔG_{rxn}	$\Delta G^{\ddagger}$	ΔG_{rxn}	$\Delta G^{\ddagger}$
0	$CH_3CH_2COOH+*\rightarrow CH_3CH_2COOH*$	0.94	N/A	0.88	N/A	0.95	N/A	0.89	N/A
1	$CH_3CH_2COOH* + 3*\rightarrow CH_3CH_2CO*** + OH*$	0.35	1.65	0.40	1.63	0.36	1.64	0.39	1.67
2	$CH_3CH_2COOH* + 2*\rightarrow CH_3CHCOOH** + H*$	-0.11	1.37	-0.20	1.30	-0.13	1.37	-0.13	1.37
3	$CH_3CH_2CO*** \rightarrow CH_3CH_2* + CO* + *$	-0.66	1.77	-0.75	1.77	-0.70	1.79	-0.71	1.79
4	$CH_3CH_2CO*** \rightarrow CH_3CHCO** + H*$	0.02	1.60	-0.04	1.53	0.01	1.61	0.00	1.59
5	$CH_3CHCOOH** + *\rightarrow CH_3CHCO** + OH*$	0.47	1.63	0.56	1.70	0.50	1.63	0.52	1.68
6	$CH_3CHCOOH** + 2*\rightarrow CH_2CHCOOH*** + H*$	-0.35	1.33	-0.31	1.33	-0.35	1.37	-0.34	1.36
7	$CH_3CHCOOH** + 2*\rightarrow CH_3CCOOH*** + H*$	-0.06	1.90	-0.05	1.91	-0.08	1.92	-0.09	1.91
8	$CH_3CHCO** + * \rightarrow CH_3CH** + CO*$	-0.84	1.77	-0.91	1.77	-0.88	1.77	-0.89	1.77
9	$CH_3CHCO** + 2*\rightarrow CH_3CCO*** + H*$	-0.39	1.37	-0.41	1.35	-0.40	1.36	-0.41	1.36
10	$CH_3CHCO** + 2*\rightarrow CH_2CHCO*** + H*$	-0.29	1.33	-0.32	1.27	-0.29	1.34	-0.29	1.32
11	$CH_2CHCOOH*** + *\rightarrow CH_2CHCO*** + OH*$	0.53	2.52	0.54	2.53	0.56	2.54	0.56	2.54
12	$CH_2CHCOOH*** + *\rightarrow CHCHCOOH*** + H*$	0.04	2.02	-0.03	1.95	0.03	2.01	0.01	1.99
13	$CH_3CCOOH*** + *\rightarrow CH_3CCO*** + OH*$	0.14	2.13	0.19	2.17	0.18	2.16	0.20	2.18
14	$CH_3CCO***\rightarrow CH_3C* + CO* + *$	-1.37	1.23	-1.43	1.23	-1.41	1.24	-1.42	1.24
15	$CH_2CHCO*** + *\rightarrow CH_2CH*** + CO*$	-0.80	1.56	-0.86	1.55	-0.86	1.56	-0.87	1.56
16	$CH_2CHCO*** + 2*\rightarrow CHCHCO**** + H*$	0.02	1.44	-0.01	1.43	0.00	1.44	0.00	1.43
17	$CHCHCOOH*** + 2*\rightarrow CHCHCO**** + OH*$	0.51	1.83	0.57	1.88	0.53	1.82	0.55	1.86
18	$CHCHCO**** \rightarrow CHCH*** + CO*$	-1.13	0.96	-1.19	1.00	-1.18	0.96	-1.18	0.97
19	$CHCH*** + H*\rightarrow CH_2CH*** + *$	0.31	1.71	0.34	1.73	0.31	1.72	0.32	1.72
20	$CH_2CH*** + H* \rightarrow CH_2CH_2** + 2*$	-0.03	1.64	0.00	1.64	-0.02	1.65	-0.01	1.64
21	$CH_2CH***\rightarrow CH_2C** + H*$	-0.43	1.21	-0.45	1.20	-0.43	1.20	-0.44	1.20
22	$CH_2C** + H*\rightarrow CH_3C* + 2*$	-0.24	1.63	-0.21	1.63	-0.23	1.64	-0.22	1.63
23	$CH_2CH*** + H* \rightarrow CH_3CH** + 2*$	-0.26	1.30	-0.27	1.27	-0.27	1.28	-0.27	1.28
24	$CH_3C* + H* \rightarrow CH_3CH**$	0.92	1.85	0.93	1.85	0.93	1.86	0.94	1.86
25	$CH_3CH** + H* \rightarrow CH_3CH_2* + 2*$	0.16	1.63	0.20	1.65	0.17	1.64	0.18	1.64
26	$CH_3CH_2* + H* \rightarrow CH_3CH_3* + *$	0.05	1.40	0.05	1.41	0.04	1.41	0.04	1.41
27	$CH_3CH_2* + 2* \rightarrow CH_2CH_2** + H*$	-0.45	1.18	-0.43	1.16	-0.44	1.18	-0.44	1.17
28	$CH_3CH_2COOH* + 2* \rightarrow CH_3CH_2COO** + H*$	-0.40	1.11	-0.34	1.14	-0.44	1.09	-0.39	1.13
29	$CH_3CH_2COO** \rightarrow CH_3CH_2* + CO_2*$	0.18	2.17	0.22	2.10	0.22	2.16	0.23	2.15
30	$CH_3CH_2COO** + 2* \rightarrow CH_3CHCOO*** + H*$	0.39	1.99	0.22	1.75	0.37	1.94	0.34	1.89
31	$CH_3CHCOOH** + * \rightarrow CH_3CHCOO** + H*$	0.10	1.55	0.08	1.60	0.06	1.54	0.09	1.58
32	$CH_3CHCOO*** + * \rightarrow CH_3CCOO*** + H*$	0.28	2.14	0.29	2.16	0.30	2.14	0.29	2.14
33	$CH_3CHCOO*** \rightarrow CH_3CH** + CO_2*$	-0.37	1.70	-0.20	1.75	-0.32	1.71	-0.29	1.72
34	$CH_3CHCOO*** + * \rightarrow CH_3CCOO*** + H*$	-0.07	1.61	-0.15	1.51	-0.12	1.57	-0.14	1.55
35	$CH_3CCOOH*** + * \rightarrow CH_3CCOO*** + H*$	0.04	1.65	-0.06	1.62	-0.01	1.64	0.00	1.67
36	$CH_3CCOOH*** \rightarrow CH_3C* + COOH**$	-0.58	1.66	-0.60	1.64	-0.55	1.68	-0.56	1.68
37	$CH_2CHCOOH*** + * \rightarrow CH_2CH*** + COOH*$	0.70	2.84	0.65	2.79	0.70	2.83	0.68	2.82
38	$CH_3CCOO*** \rightarrow CH_3C* + CO_2* + *$	-1.12	1.40	-0.89	1.59	-1.05	1.46	-1.00	1.50
39	$COOH** \rightarrow CO_2* + H*$	-0.55	1.12	-0.41	1.09	-0.56	1.03	-0.49	1.08
40	$COOH** \rightarrow CO* + OH*$	-0.65	1.17	-0.64	1.16	-0.68	1.13	-0.66	1.16
41	$OH* + H* \rightarrow H_2O* + *$	-0.20	1.45	-0.15	1.44	-0.20	1.43	-0.18	1.45

Table 1. (Continued)
Note: * symbolizes a free site.

#	Reaction	Gas		Water		Octane		Butanol	
		ΔG_{rxn}	$\Delta G^{\ddagger}$	ΔG_{rxn}	$\Delta G^{\ddagger}$	ΔG_{rxn}	$\Delta G^{\ddagger}$	ΔG_{rxn}	$\Delta G^{\ddagger}$
42	$CH_3CH_3^* \rightarrow CH_3CH_3 + *$	-0.79	N/A	-0.81	N/A	-0.78	N/A	-0.78	N/A
43	$CH_2CH_2^{**} \rightarrow CH_2CH_2 + 2*$	0.01	N/A	-0.01	N/A	0.00	N/A	0.00	N/A
44	$H_2O^* \rightarrow H_2O + *$	-0.49	N/A	-0.37	N/A	-0.50	N/A	-0.44	N/A
45	$CO_2^* \rightarrow CO_2 + *$	-0.81	N/A	-0.83	N/A	-0.81	N/A	-0.81	N/A
46	$CHCH^* \rightarrow CHCH + *$	1.16	N/A	1.17	N/A	1.14	N/A	1.15	N/A

Table 2. Equilibrium and forward rate constants for the elementary steps in the HDO of propanoic acid over Pd (111) model surfaces at a temperature of 473 K.

Reaction #	Gas		Water		Octane		Butanol	
	K_{eq}	$k_{forward}$ (s^{-1})	K_{eq}	$k_{forward}$ (s^{-1})	K_{eq}	$k_{forward}$ (s^{-1})	K_{eq}	$k_{forward}$ (s^{-1})
0	8.98×10^{-11}	9.52×10^{7}	4.45×10^{-10}	9.52×10^{7}	8.46×10^{-11}	9.52×10^{7}	3.68×10^{-10}	9.52×10^{7}
1	2.10×10^{-4}	3.14×10^{3}	5.18×10^{-5}	6.36×10^{3}	1.45×10^{-4}	4.66×10^{3}	7.83×10^{-5}	2.37×10^{3}
2	1.39×10^{1}	3.04×10^{6}	1.30×10^{2}	2.08×10^{7}	2.17×10^{1}	3.75×10^{6}	2.59×10^{1}	4.87×10^{6}
3	1.01×10^{7}	1.76×10^{2}	9.71×10^{7}	1.99×10^{2}	2.54×10^{7}	1.07×10^{2}	3.37×10^{7}	1.17×10^{2}
4	6.05×10^{-1}	1.34×10^{4}	2.76	6.66×10^{4}	7.41×10^{-1}	9.57×10^{3}	9.90×10^{-1}	1.35×10^{4}
5	9.14×10^{-6}	6.16×10^{3}	1.10×10^{-6}	1.02×10^{3}	4.94×10^{-6}	5.78×10^{3}	2.99×10^{-6}	1.70×10^{3}
6	5.81×10^{3}	8.43×10^{6}	1.87×10^{3}	8.74×10^{6}	4.96×10^{3}	3.70×10^{6}	3.87×10^{3}	4.41×10^{6}
7	4.06	6.85	3.03	6.08	7.88	5.21	8.24	5.86
8	8.58×10^{8}	2.03×10^{2}	5.22×10^{9}	1.66×10^{2}	2.28×10^{9}	2.04×10^{2}	2.75×10^{9}	1.98×10^{2}
9	1.32×10^{4}	3.51×10^{6}	2.52×10^{4}	5.78×10^{6}	2.00×10^{4}	4.17×10^{6}	2.17×10^{4}	4.39×10^{6}
10	1.33×10^{3}	8.80×10^{6}	2.68×10^{3}	3.82×10^{7}	1.11×10^{3}	6.29×10^{6}	1.33×10^{3}	1.05×10^{7}
11	2.09×10^{-6}	1.68	1.57×10^{-6}	6.52	1.11×10^{-6}	3.20	1.03×10^{-6}	2.55
12	4.16×10^{-1}	3.31×10^{3}	2.15	1.57×10^{4}	4.58×10^{-1}	3.40×10^{3}	7.55×10^{-1}	5.52×10^{3}
13	2.98×10^{-2}	6.70×10^{4}	9.13×10^{-3}	6.96×10^{4}	1.26×10^{-2}	4.53×10^{4}	7.88×10^{-3}	2.18×10^{4}
14	3.95×10^{14}	9.98×10^{7}	1.71×10^{15}	1.15×10^{8}	1.03×10^{15}	7.62×10^{7}	1.23×10^{15}	8.07×10^{7}
15	3.52×10^{8}	2.91×10^{4}	1.57×10^{9}	3.59×10^{4}	1.61×10^{9}	3.08×10^{4}	1.74×10^{9}	3.22×10^{4}
16	6.61×10^{-1}	5.57×10^{5}	1.28	7.05×10^{5}	9.61×10^{-1}	6.46×10^{5}	1.09	6.96×10^{5}
17	3.32×10^{-6}	4.33×10^{1}	9.37×10^{-7}	1.35×10^{1}	2.33×10^{-6}	4.77×10^{1}	1.48×10^{-6}	1.95×10^{1}
18	1.12×10^{12}	8.65×10^{10}	4.63×10^{12}	3.07×10^{10}	3.38×10^{12}	7.58×10^{10}	3.86×10^{12}	6.36×10^{10}
19	4.76×10^{-4}	8.33×10^{2}	2.65×10^{-4}	4.63×10^{2}	4.96×10^{-4}	6.37×10^{2}	4.14×10^{-4}	6.02×10^{2}
20	2.28	4.99×10^{3}	9.49×10^{-1}	4.97×10^{3}	1.48	3.86×10^{3}	1.26	3.96×10^{3}
21	3.39×10^{4}	1.73×10^{8}	6.28×10^{4}	2.10×10^{8}	4.21×10^{4}	1.99×10^{8}	4.72×10^{4}	2.05×10^{8}
22	3.30×10^{2}	5.89×10^{3}	1.63×10^{2}	6.28×10^{3}	2.74×10^{2}	4.46×10^{3}	2.45×10^{2}	5.09×10^{3}
23	5.46×10^{2}	1.94×10^{7}	8.06×10^{2}	3.68×10^{7}	7.86×10^{2}	2.73×10^{7}	8.41×10^{2}	3.19×10^{7}
24	1.64×10^{-10}	2.51×10^{1}	1.21×10^{-10}	2.31×10^{1}	1.10×10^{-10}	1.87×10^{1}	1.03×10^{-10}	1.81×10^{1}
25	1.95×10^{-2}	5.46×10^{3}	6.75×10^{-3}	3.93×10^{3}	1.50×10^{-2}	4.65×10^{3}	1.24×10^{-2}	4.62×10^{3}
26	3.17×10^{-1}	1.46×10^{6}	2.65×10^{-1}	1.29×10^{6}	4.01×10^{-1}	1.37×10^{6}	3.62×10^{-1}	1.36×10^{6}
27	6.40×10^{4}	3.26×10^{8}	3.61×10^{4}	5.39×10^{8}	5.30×10^{4}	3.74×10^{8}	4.80×10^{4}	4.10×10^{8}
28	1.92×10^{4}	1.99×10^{9}	3.83×10^{3}	8.79×10^{8}	4.64×10^{4}	3.62×10^{9}	1.33×10^{4}	1.25×10^{9}
29	1.08×10^{-2}	1.13×10^{-2}	4.28×10^{-3}	5.41×10^{-2}	4.29×10^{-3}	1.25×10^{-2}	3.88×10^{-3}	1.57×10^{-2}
30	6.55×10^{-5}	9.39×10^{-1}	4.50×10^{-3}	3.29×10^{2}	1.07×10^{-4}	2.84	2.38×10^{-4}	1.04×10^{1}
31	9.04×10^{-2}	3.95×10^{4}	1.33×10^{-1}	1.11×10^{4}	2.29×10^{-1}	5.08×10^{4}	1.22×10^{-1}	1.89×10^{4}
32	9.80×10^{-4}	2.33×10^{-2}	8.03×10^{-4}	1.22×10^{-2}	5.97×10^{-4}	1.90×10^{-2}	8.03×10^{-4}	1.96×10^{-2}
33	8.49×10^{3}	1.05×10^{3}	1.41×10^{2}	3.13×10^{2}	2.66×10^{3}	7.34×10^{2}	1.32×10^{3}	5.81×10^{2}
34	6.23	8.87×10^{3}	4.27×10^{1}	1.11×10^{5}	1.89×10^{1}	2.40×10^{4}	3.02×10^{1}	4.54×10^{4}
35	3.43×10^{-1}	3.29×10^{3}	4.60	7.30×10^{3}	1.36	3.96×10^{3}	1.10	2.27×10^{3}
36	1.47×10^{6}	2.84×10^{3}	2.19×10^{6}	4.52×10^{3}	6.88×10^{5}	1.58×10^{3}	9.46×10^{5}	1.72×10^{3}
37	3.33×10^{-8}	7.99×10^{-10}	1.25×10^{-7}	2.79×10^{-9}	3.42×10^{-8}	9.18×10^{-10}	6.30×10^{-8}	1.20×10^{-9}
38	9.13×10^{11}	1.76×10^{6}	3.01×10^{9}	1.68×10^{4}	1.40×10^{11}	3.60×10^{5}	4.66×10^{10}	1.32×10^{5}
39	7.28×10^{5}	1.63×10^{9}	2.16×10^{4}	3.18×10^{9}	9.49×10^{5}	1.45×10^{10}	1.86×10^{5}	4.57×10^{9}
40	8.00×10^{6}	4.84×10^{8}	7.13×10^{6}	5.36×10^{8}	1.89×10^{7}	1.23×10^{9}	1.02×10^{7}	5.54×10^{8}
41	1.48×10^{2}	4.20×10^{5}	3.75×10^{1}	5.44×10^{5}	1.53×10^{2}	7.96×10^{5}	8.07×10^{1}	4.23×10^{5}

Table 2. (Continued)

Reaction #	Gas		Water		Octane		Butanol	
	K_{eq}	$k_{forward}$ (s^{-1})	K_{eq}	$k_{forward}$ (s^{-1})	K_{eq}	$k_{forward}$ (s^{-1})	K_{eq}	$k_{forward}$ (s^{-1})
42	2.44×10^{8}	3.65×10^{16}	4.54×10^{8}	6.79×10^{16}	1.94×10^{8}	2.91×10^{16}	2.12×10^{8}	3.17×10^{16}
43	7.22×10^{-1}	1.12×10^{8}	1.17	1.81×10^{8}	9.66×10^{-1}	1.50×10^{8}	9.53×10^{-1}	1.48×10^{8}
44	1.73×10^{5}	3.35×10^{13}	9.36×10^{3}	1.81×10^{12}	2.12×10^{5}	4.10×10^{13}	4.54×10^{4}	9.45×10^{12}
45	2.50×10^{8}	3.24×10^{16}	4.11×10^{8}	5.32×10^{16}	2.75×10^{8}	3.56×10^{16}	2.48×10^{8}	3.21×10^{16}
46	1.60×10^{-6}	9.98×10^{-15}	1.30×10^{-6}	8.09×10^{-15}	2.73×10^{-6}	1.70×10^{-14}	2.10×10^{-6}	1.31×10^{-14}

Figure 1. Network of elementary reaction steps considered in the hydrodeoxygenation of propanoic acid over Pd (111). Elementary reactions involved in the DCX mechanism are shown with blue color arrows, DCN reactions are illustrated with red color arrows, and those reaction involved in both mechanisms such as dehydrogenation reactions and removal of the hydrocarbon pool are shown with gray color arrows.

Figure 2. TOFs (s^{-1}) for various elementary steps in the HDO of propanoic acid in absence of any solvents at a temperature of 473 K and a propanoic acid gas phase pressure of 1 bar and a hydrogen partial pressure of 1 bar or 0.001 bar (numbers inside the square brackets []). All other reaction conditions are given in section 3.1. Elementary reactions involved in the DCX mechanism are shown with blue color arrows, DCN reactions are illustrated with red color arrows, and those reaction involved in both mechanisms such as dehydrogenation reactions and removal of the hydrocarbon pool are shown with gray color arrows. Elementary reactions involved in the most dominant reaction pathway are illustrated with double-line arrows. The overall TOF_{DCN} was calculated to be 1.28×10^{-6} s^{-1} [2.11×10^{-5} s^{-1}] while the TOF_{DCX} was 2.26×10^{-8} s^{-1} [1.43×10^{-7} s^{-1}] (TOF_{DCN}/TOF_{DCX} = 56.4 [148]).

Figure 3. TOFs (s^{-1}) for various elementary steps in the HDO of propanoic acid in the presence of liquid water at a temperature of 473 K and a chemical potential corresponding to a propanoic acid gas phase pressure of 1 bar and a hydrogen partial pressure of 1 bar or 0.001 bar (numbers inside the square brackets []). All other reaction conditions are given in section 3.1. Elementary reactions involved in the DCX mechanism are shown with blue color arrows, DCN reactions are illustrated with red color arrows, and those reaction involved in both mechanisms such as dehydrogenation reactions and removal of the hydrocarbon pool are shown with gray color arrows. Elementary reactions involved in the most dominant reaction pathway are illustrated with double-line arrows. The overall TOF_{DCN} was calculated to be 3.00×10^{-5} s^{-1} [2.94×10^{-4} s^{-1}] while the TOF_{DCX} was = 6.21×10^{-6} s^{-1} [7.86×10^{-5} s^{-1}] (TOF_{DCN}/TOF_{DCX} = 4.8 [3.7]).

Figure 4. TOFs (s^{-1}) for various elementary steps in the HDO of propanoic acid in the presence of n-octane at a temperature of 473 K and a chemical potential corresponding to a propanoic acid gas phase pressure of 1 bar and a hydrogen partial pressure of 1 bar or 0.001 bar (numbers inside the square brackets []). All

other reaction conditions are given in section 3.1. Elementary reactions involved in the DCX mechanism are shown with blue color arrows, DCN reactions are illustrated with red color arrows, and those reaction involved in both mechanisms such as dehydrogenation reactions and removal of the hydrocarbon pool are shown with gray color arrows. Elementary reactions involved in the most dominant reaction pathway are illustrated with double-line arrows. The overall TOF_{DCN} was calculated to be 1.64×10^{-6} s^{-1} [2.23×10^{-5} s^{-1}] while the TOF_{DCX} was 1.28×10^{-7} s^{-1} [1.14×10^{-6} s^{-1}] (TOF_{DCN}/TOF_{DCX} = 12.8 [19.6]).

Figure 5. TOFs (s^{-1}) for various elementary steps in the HDO of propanoic acid in the presence of n-butanol at a temperature of 473 K, a chemical potential corresponding to a propanoic acid gas phase pressure of 1 bar and a hydrogen partial pressure of 1 bar or 0.001 bar (numbers inside the square brackets []). All other reaction conditions are given in section 3.1. Elementary reactions involved in the DCX mechanism are shown with blue color arrows, DCN reactions are illustrated with red color arrows, and those reaction involved in both mechanisms such as dehydrogenation reactions and removal of the hydrocarbon pool are shown with gray color arrows. Elementary reactions involved in the most dominant reaction pathway are illustrated with double-line arrows. The overall TOF_{DCN} was calculated to be 5.12×10^{-6} s^{-1} [5.86×10^{-5} s^{-1}] while the TOF_{DCX} was 6.26×10^{-7} s^{-1} [6.76×10^{-6} s^{-1}] (TOF_{DCN}/TOF_{DCX} = 8.2 [8.7]).

Figure 1

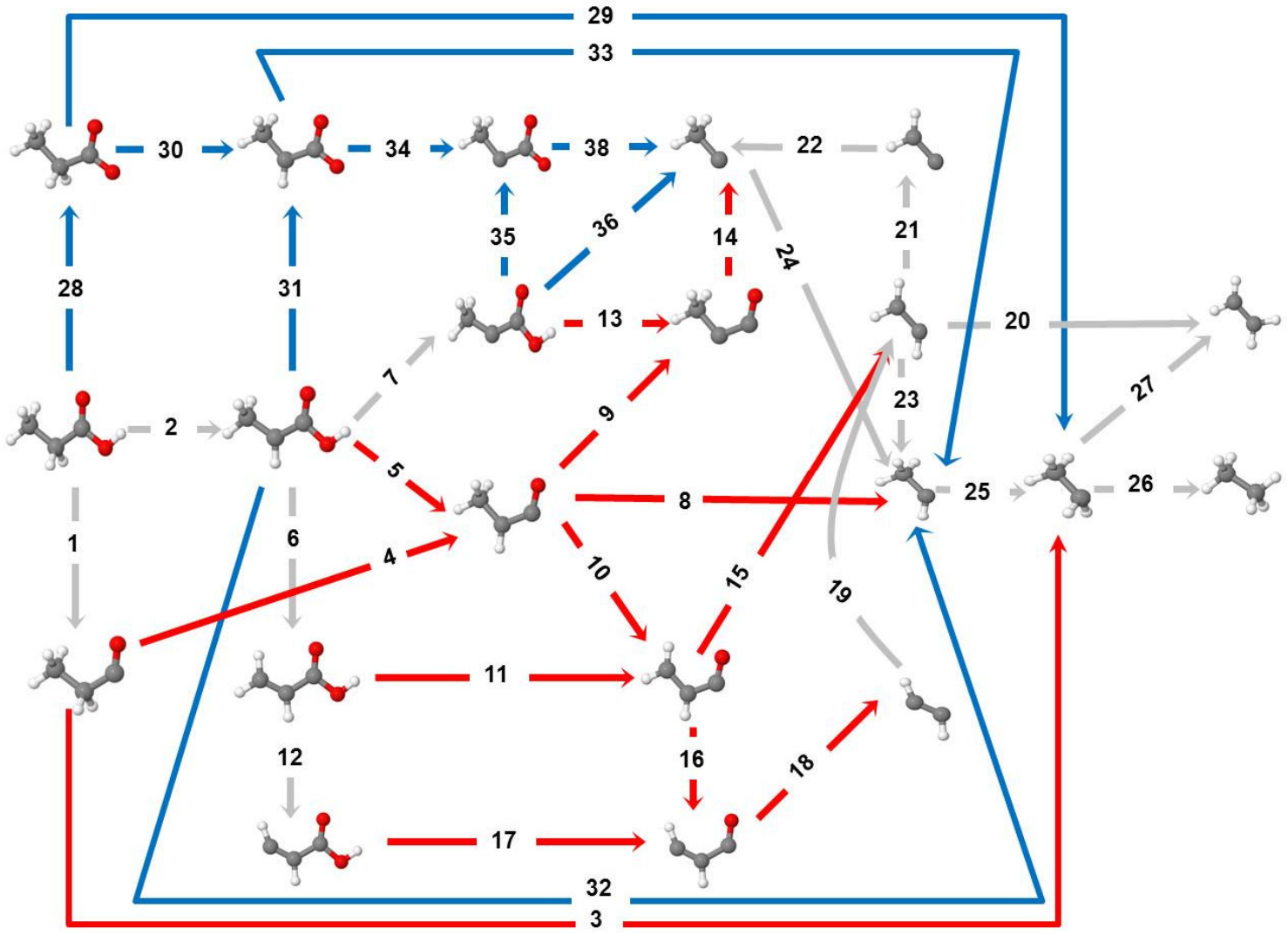
29
33
30
34
38
22
28
31
35
36
14
24
21
13
20
2
7
9
23
27
5
8
25
26
1
6
4
10
15
19
11
12
16
18
17
32
3

Figure 2

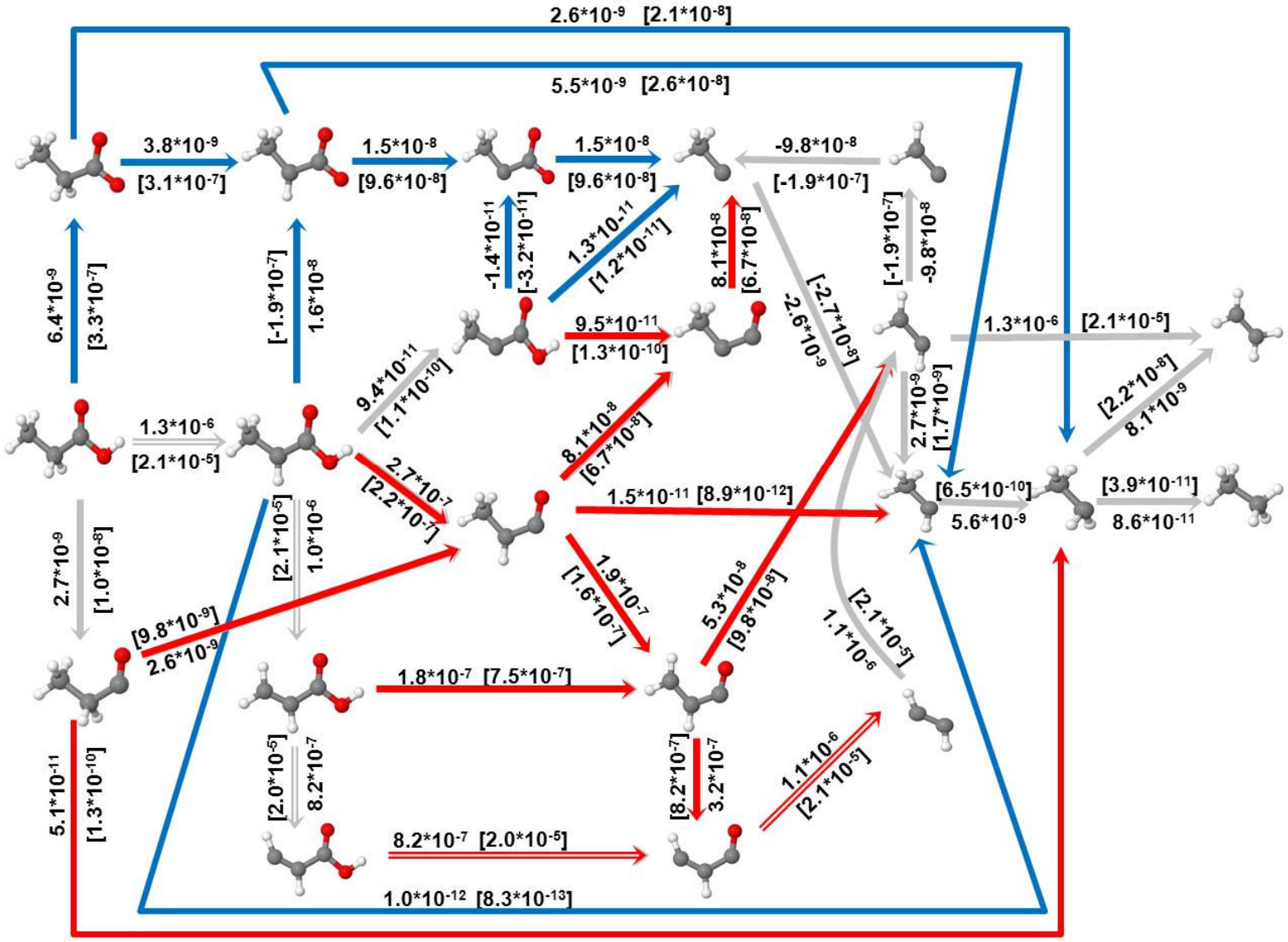
2.6*10-9 [2.1*10-8]
5.5*10-9 [2.6*10-8]
3.8*10-9
[3.1*10-7]
1.5*10-8
[9.6*10-8]
1.5*10-8
[9.6*10-8]
-9.8*10-8
[-1.9*10-7]
6.4*10-9
[3.3*10-7]
[-1.9*10-7]
1.6*10-8
-1.4*10-11
[-3.2*10-11]
1.3*10-11
[1.2*10-11]
8.1*10-8
[6.7*10-8]
[-2.7*10-8]
-2.6*10-9
[-1.9*10-7]
-9.8*10-8
1.3*10-6
[2.1*10-5]
9.4*10-11
[1.1*10-10]
9.5*10-11
[1.3*10-10]
2.7*10-9
[1.7*10-9]
[2.2*10-8]
8.1*10-9
1.3*10-6
[2.1*10-5]
8.1*10-8
[6.7*10-8]
2.7*10-7
[2.2*10-7]
1.5*10-11 [8.9*10-12]
[6.5*10-10]
5.6*10-9
[3.9*10-11]
8.6*10-11
2.7*10-9
[1.0*10-8]
[2.1*10-5]
1.0*10-6
1.9*10-7
[1.6*10-7]
5.3*10-8
[9.8*10-8]
[2.1*10-5]
1.1*10-6
[9.8*10-9]
2.6*10-9
1.8*10-7 [7.5*10-7]
5.1*10-11
[1.3*10-10]
[2.0*10-5]
8.2*10-7
[8.2*10-7]
3.2*10-7
1.1*10-6
[2.1*10-5]
8.2*10-7 [2.0*10-5]
1.0*10-12 [8.3*10-13]

Figure 3

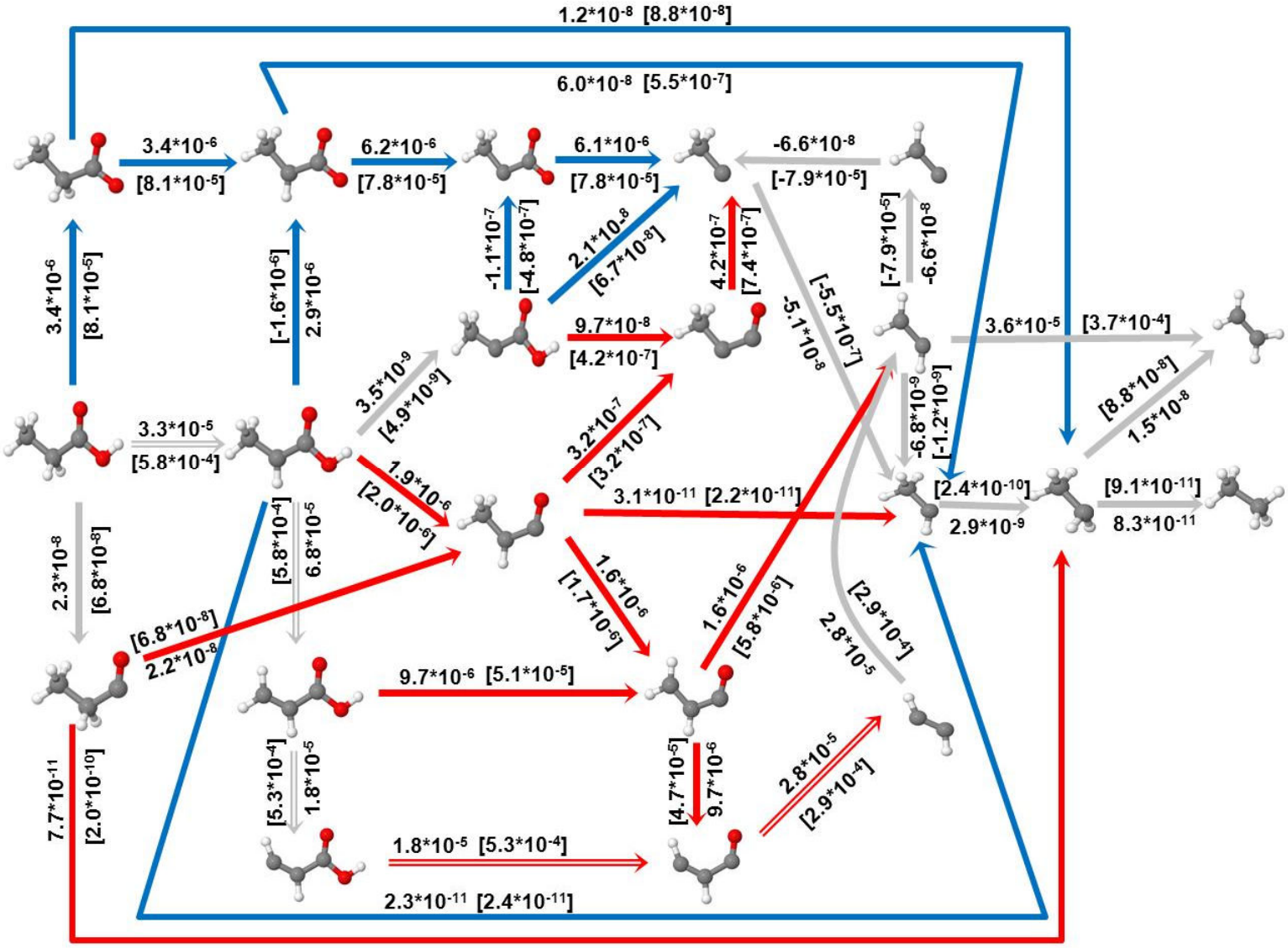
1.2*10-8 [8.8*10-8]
6.0*10-8 [5.5*10-7]
3.4*10-6
[8.1*10-5]
6.2*10-6
[7.8*10-5]
6.1*10-6
[7.8*10-5]
-6.6*10-8
[-7.9*10-5]
3.4*10-6
[8.1*10-5]
[-1.6*10-6]
2.9*10-6
-1.1*10-7
[-4.8*10-7]
2.1*10-8
[6.7*10-8]
4.2*10-7
[7.4*10-7]
[-7.9*10-5]
-6.6*10-8
9.7*10-8
[4.2*10-7]
-5.1*10-8
[-5.5*10-7]
3.6*10-5
[3.7*10-4]
3.5*10-9
[4.9*10-9]
3.3*10-5
[5.8*10-4]
3.2*10-7
[3.2*10-7]
-6.8*10-9
[-1.2*10-9]
[8.8*10-8]
1.5*10-8
1.9*10-6
[2.0*10-6]
3.1*10-11 [2.2*10-11]
[2.4*10-10]
2.9*10-9
[9.1*10-11]
8.3*10-11
2.3*10-8
[6.8*10-8]
[5.8*10-4]
6.8*10-5
1.6*10-6
[1.7*10-6]
1.6*10-6
[5.8*10-6]
[2.9*10-4]
2.8*10-5
[6.8*10-8]
2.2*10-8
9.7*10-6 [5.1*10-5]
7.7*10-11
[2.0*10-10]
[5.3*10-4]
1.8*10-5
[4.7*10-5]
9.7*10-6
2.8*10-5
[2.9*10-4]
1.8*10-5 [5.3*10-4]
2.3*10-11 [2.4*10-11]

Figure 4

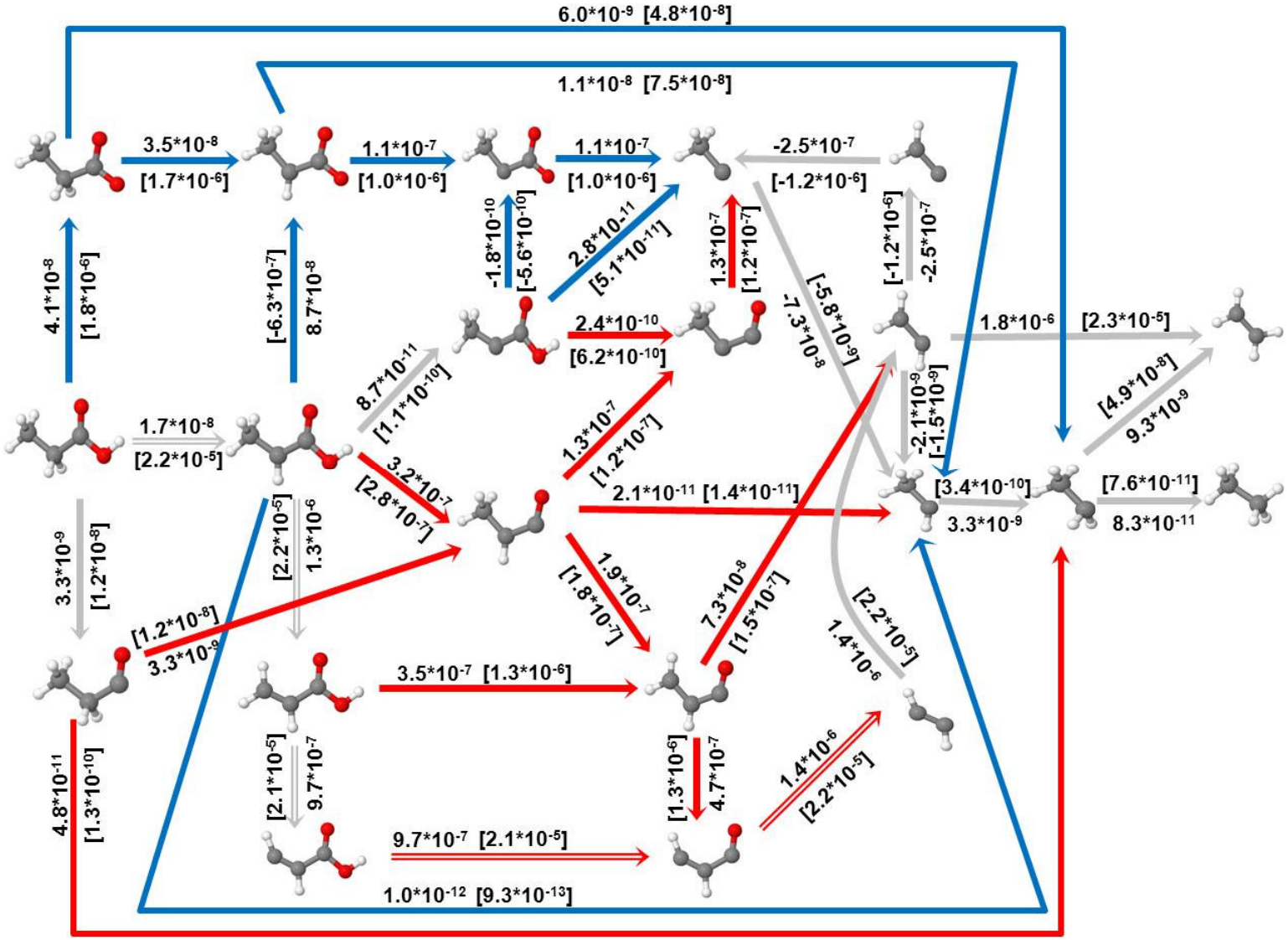
6.0*10-9 [4.8*10-8]
1.1*10-8 [7.5*10-8]
3.5*10-8
[1.7*10-6]
1.1*10-7
[1.0*10-6]
1.1*10-7
[1.0*10-6]
-2.5*10-7
[-1.2*10-6]
4.1*10-8
[1.8*10-6]
[-6.3*10-7]
8.7*10-8
-1.8*10-10
[-5.6*10-10]
2.8*10-11
[5.1*10-11]
1.3*10-7
[1.2*10-7]
[-1.2*10-6]
-2.5*10-7
[-5.8*10-9]
-7.3*10-8
1.8*10-6
[2.3*10-5]
2.4*10-10
[6.2*10-10]
8.7*10-11
[1.1*10-10]
1.7*10-8
[2.2*10-5]
1.3*10-7
[1.2*10-7]
-2.1*10-9
[-1.5*10-9]
[4.9*10-8]
9.3*10-9
3.2*10-7
[2.8*10-7]
2.1*10-11 [1.4*10-11]
[3.4*10-10]
3.3*10-9
[7.6*10-11]
8.3*10-11
3.3*10-9
[1.2*10-8]
[2.2*10-5]
1.3*10-6
[1.2*10-8]
3.3*10-9
1.9*10-7
[1.8*10-7]
7.3*10-8
[1.5*10-7]
[2.2*10-5]
1.4*10-6
3.5*10-7 [1.3*10-6]
4.8*10-11
[1.3*10-10]
[2.1*10-5]
9.7*10-7
[1.3*10-6]
4.7*10-7
1.4*10-6
[2.2*10-5]
9.7*10-7 [2.1*10-5]
1.0*10-12 [9.3*10-13]

Figure 5

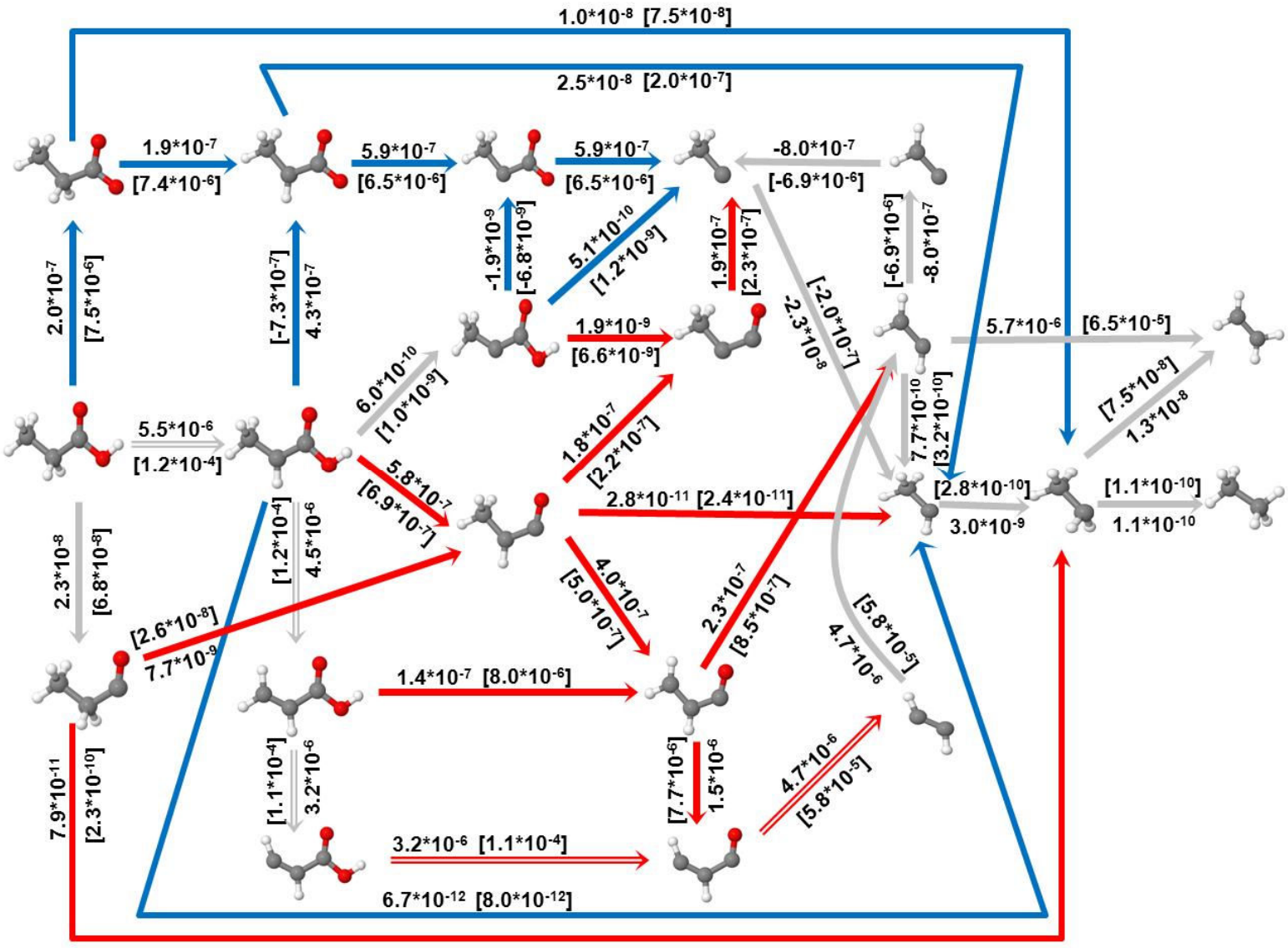
1.0*10-8 [7.5*10-8]
2.5*10-8 [2.0*10-7]
1.9*10-7
[7.4*10-6]
5.9*10-7
[6.5*10-6]
5.9*10-7
[6.5*10-6]
-8.0*10-7
[-6.9*10-6]
2.0*10-7
[7.5*10-6]
[-7.3*10-7]
4.3*10-7
-1.9*10-9
[-6.8*10-9]
5.1*10-10
[1.2*10-9]
1.9*10-7
[2.3*10-7]
[-6.9*10-6]
-8.0*10-7
[-2.0*10-7]
-2.3*10-8
5.7*10-6
[6.5*10-5]
1.9*10-9
[6.6*10-9]
6.0*10-10
[1.0*10-9]
5.5*10-6
[1.2*10-4]
1.8*10-7
[2.2*10-7]
5.8*10-7
[6.9*10-7]
2.8*10-11 [2.4*10-11]
7.7*10-10
[3.2*10-10]
[7.5*10-8]
1.3*10-8
[2.8*10-10]
3.0*10-9
[1.1*10-10]
1.1*10-10
2.3*10-8
[6.8*10-8]
[1.2*10-4]
4.5*10-6
[2.6*10-8]
7.7*10-9
4.0*10-7
[5.0*10-7]
2.3*10-7
[8.5*10-7]
[5.8*10-5]
4.7*10-6
1.4*10-7 [8.0*10-6]
7.9*10-11
[2.3*10-10]
[1.1*10-4]
3.2*10-6
[7.7*10-6]
1.5*10-6
4.7*10-6
[5.8*10-5]
3.2*10-6 [1.1*10-4]
6.7*10-12 [8.0*10-12]